Generative Adversarial Learning of Sinkhorn Algorithm Initializations

Jonathan Geuter 1 Vaios Laschos 2

Abstract

The Sinkhorn algorithm (Cuturi, 2013) is the stateof-the-art to compute approximations of optimal transport distances between discrete probability distributions, making use of an entropically regularized formulation of the problem. The algorithm is guaranteed to converge, no matter its initialization. This lead to little attention being paid to initializing it, and simple starting vectors like the n-dimensional one-vector are common choices. We train a neural network to compute initializations for the algorithm, which significantly outperform standard initializations. The network predicts a potential of the optimal transport dual problem, where training is conducted in an adversarial fashion using a second, generating network. The network is universal in the sense that it is able to generalize to any pair of distributions of fixed dimension after training, and we prove that the generating network is universal in the sense that it is capable of producing any pair of distributions during training. Furthermore, we show that for certain applications the network can be used independently.

1. Introduction

Optimal Transport (Villani, 2009; Peyré & Cuturi, 2019) plays an increasing role in various areas. Besides economics (Galichon, 2016), it thrives in machine learning applications, and has been used in domain adaptation (Courty et al., 2017), single-cell genomics (Schiebinger et al., 2019), imitation learning (Dadashi et al., 2020), imaging (Schmitz et al., 2018) and signal processing (Kolouri et al., 2017). The discrete optimal transport problem can be solved as a linear program; however, this approach proves to be prohibitively expensive, particularly in high dimensions. Adding an entropic regularizer to the problem, one can solve it using the well-known Sinkhorn algorithm (Cuturi, 2013), which is

computationally efficient, more robust to outliers, differentiable, and easily parallelizable. Furthermore, it is guaranteed to converge to the solution of the entropic problem, which is unique by strict convexity of the problem. Hence, little attention has been paid to initializing the Sinkhorn algorithm. We will show that good initializations can speed up the algorithm significantly. To this end, we learn initializations to the algorithm with a neural network, which, given two distributions, predicts a potential of the optimal transport dual problem, which is closely linked to the limit point of the Sinkhorn algorithm. In Section 5, we will see that for certain problems, the network can also be used independently as an approximation function of optimal dual potentials. Importantly, this approach preserves all the important advantages of the Sinkhorn algorithm, such as efficiency, differentiability, and parallelizability.

Training will be supervised, where the true potential is computed for each training sample. The crucial question is: What is the best way to generate training samples? The training dataset needs to be rich enough to allow the network to generalize to any dataset during testing. We tackle this issue with a two-network approach, where one network (the generator) learns to generate training samples from a Gaussian prior while the other network (the approximator) learns to predict dual potentials given the generating network's outputs. The generator, denoted by g_{θ} with parameters θ , is a one-layer ResNet (He et al., 2016), and we prove that it is capable of generating any pair of distributions; in fact, this result is proven for a far more general class of ResNets. The approximator, denoted by h_{ϕ} with parameters ϕ , is a three-layer fully connected network. The networks will be trained in an adversarial fashion, similar to a GAN, where the generator's loss is negative the approximator's loss. The generator and approximator will be trained in alternation, such that the generator consistently aims at producing those samples which the approximator has most problems with. To our knowledge, this is the first universal approach to initializing the Sinkhorn algorithm.

2. Related Work

Initializing Sinkhorn. There exists very little literature on initializing the Sinkhorn algorithm. (Thornton & Cuturi, 2022) propose using dual vectors recovered from the un-

¹Department of Mathematics, Technische Universität Berlin, Germany ²Weierstrass Institute, Berlin, Germany. Correspondence to: Jonathan Geuter <jonathan.geuter at gmx.de>.

regularized 1D optimal transport problem, or from known transport maps in a Gaussian setup, and were able to significantly speed up convergence. In (Amos et al., 2022), a learned approach is taken as well. However, the authors restrict themselves to the case of particular datasets such as MNIST, on which both training and testing is performed. They also do not use a generator in their training. Furthermore, the loss function they use for the approximator on a sample of two distributions (μ, ν) is

$$loss(\boldsymbol{\mu}, \boldsymbol{\nu}) = -(\langle net(\boldsymbol{\mu}, \boldsymbol{\nu}), \boldsymbol{\mu} \rangle + \langle net(\boldsymbol{\mu}, \boldsymbol{\nu})^C, \boldsymbol{\nu} \rangle),$$

where $\operatorname{net}(\mu, \nu)^C$ denotes the C-transform (cmp. (Villani, 2009)), C being the cost matrix; i.e., they try to maximize the optimal transport dual, cf. section 3. This approach is more elegant than ours in the sense that it allows for unsupervised training, as no ground-truth dual potentials are needed in the training data. However, as we will see in section 5, it it significantly worse at learning to approximate potentials than our supervised approach.

Learning OT Distances. Several attempts at directly learning OT distances or maps in specific settings have been made. (Courty et al., 2018) propose learning a Wasserstein embedding, i.e. embedding distributions in Euclidean space, where the Euclidean distance mimics the Wasserstein distance. Empirically, the approach works very well for low-dimensional datasets, but there do not exist theoretical results on universal embeddability. In (Bunne et al., 2022a), transport maps between continuous input distributions conditioned on a context variable are learned. This approach builds on Input Convex Neural Networks (Amos et al., 2017). In another interesting recent paper (Gracyk & Chen, 2022), a network is trained to learn the Wasserstein geodesic between two continuous input distributions. This approach builds upon the dynamic OT formulation (Benamou & Brenier, 2000), which expresses the Wasserstein distance as a minimal kinetic energy flow through probability space. This approach was able to significantly reduce computation costs.

OT for Machine Learning. Apart from using machine learning to approximate optimal transport distances and maps, the reverse direction – leveraging OT to formulate new machine learning methods – has also seen a surge in popularity in recent years. Oftentimes, Wasserstein distances are used in loss functions as a generic tool to measure discrepancies between distributions, such as in the celebrated Wasserstein GAN (Arjovsky et al., 2017), multi-label learning (Frogner et al., 2015), inverse problems in phsyics (Engquist & Yang, 2019), or few-shot image classification to compute distances between images (Zhang et al., 2020). Another interesting application lies in the area of gradient flows, which are absolutely continuous flows along the gradient of a functional. They can be approximated using the Jordan-Kinderlehrer-Otto scheme, which involves solving

OT problems (Alvarez-Melis & Fusi, 2021; Alvarez-Melis et al., 2022; Bunne et al., 2022b).

Generative Modelling. In generative modelling, the goal is usually to find a parametrized distribution ρ_{θ} which minimizes, in some metric, the distance to a target distribution ρ_{data} . Typically, this means minimizing some functional $F(\rho_{\theta}) = d(\rho_{\theta}, \rho_{\text{data}})$, where d measures the discrepancy between the distributions, and samples from ρ_{data} are usually available. While our generator also tries to learn such a parametrized distribution ρ_{θ} , our approach differs from this framework in that we do not have access to a given target distribution. Another similarity can be found in our loss function, which resembles the loss function of Generative Adversarial Networks (Goodfellow et al., 2014), or GANs for short. Given samples $z \sim \rho_z$ from a (Gaussian) prior and samples $z \sim \rho_{\text{data}}$ from the target distribution, the GAN loss is

$$\min_{G} \max_{D} \mathbb{E}_{\boldsymbol{x} \sim \rho_{\text{data}}} \left[\log D(\boldsymbol{x}) \right] + \mathbb{E}_{\boldsymbol{z} \sim \rho_{\boldsymbol{z}}} \left[\log (1 - D(G(\boldsymbol{z}))) \right],$$

where G is the generator and D the so-called *discriminator*, which predicts the probability that a sample came from the target distribution rather than the generator. Similarly, our loss will be of the form

$$\max_{\boldsymbol{\theta}} \min_{\boldsymbol{\phi}} \mathbb{E}_{\boldsymbol{z} \sim \rho_{\boldsymbol{z}}} \left[\text{MSE} \left(h_{\boldsymbol{\phi}}(g_{\boldsymbol{\theta}}(\boldsymbol{z})), \boldsymbol{f}_{g(\boldsymbol{z})} \right) \right],$$

where $f_{g(z)}$ denotes a dual potential of the sample $(\mu, \nu) = g(z)$, and MSE denotes the mean squared error. For more details, see section 4.

Various kinds of generative models exist. Besides GANs, Variational Auto-Encoders (Kingma & Welling, 2014), and Diffusion Models (Sohl-Dickstein et al., 2015; Song & Ermon, 2019), a fast-growing line of work is that of Normalizing Flows (Dinh et al., 2015; Rezende & Mohamed, 2015; Kobyzev et al., 2021; Papamakarios et al., 2021), which are compositions of parametrized, invertible transformations pushing a (typically Gaussian) probability distribution to a target distribution. Our approach shares some common characteristics; however, we do not need invertibility, which is crucial to Normalizing Flows. This allows us to simply use a (non-invertible) ResNet as a generator instead. However, in Section 4.1 we will see that the generator can easily be made invertible by controlling the Lipschitz constant of the generator's network.

3. Optimal Transport

In this section, we recall some properties of optimal transport in the discrete case. We will write vectors in bold and matrices as capital letters. By [n] we refer to the set $\{1,2,...,n\}$. By $1_n \in \mathbb{R}^n$ we denote the vector where all entries are equal to 1. The n-1 dimensional simplex in \mathbb{R}^n will be denoted by Δ^{n-1} , and all elements in the simplex

with positive entries are denoted by $\Delta_{>0}^{n-1}$. In the following, let μ and ν be two discrete, m- resp. n-dimensional probability measures on some spaces $\mathcal{X} = \{x_1, ..., x_m\}$ and $\mathcal{Y} = \{y_1, ..., y_n\}$ equipped with the discrete topologies. We will oftentimes abuse notation by considering μ and ν to be the vectors $\begin{bmatrix} \mu_1 & \dots & \mu_m \end{bmatrix}^\top \in \Delta^{m-1}$ resp. $\begin{bmatrix} \nu_1 & \dots & \nu_n \end{bmatrix}^\top \in \Delta^{n-1}$.

3.1. Unregularized Optimal Transport

The discrete optimal transport problem, also referred to as the *Kantorovich problem*, is defined as follows.

Problem 1 (Optimal Transport Problem).

$$L(\boldsymbol{\mu}, \boldsymbol{\nu}) := \min_{\Gamma \in \Pi(\boldsymbol{\mu}, \boldsymbol{\nu})} \langle C, \Gamma \rangle$$

Here, $\Pi(\mu, \nu)$ denotes the set of all *transport plans* between μ and ν , i.e. matrices $\Gamma \in \mathbb{R}_{\geq 0}^{m \times n}$ s.t. $\Gamma 1_n = \mu$ and $\Gamma^{\top} 1_m = \nu$. The problem has a dual formulation:

Problem 2 (Dual Optimal Transport Problem).

$$D(\boldsymbol{\mu}, \boldsymbol{\nu}) := \max_{\substack{\boldsymbol{f} \in \mathbb{R}^m, \ \boldsymbol{g} \in \mathbb{R}^n \\ \boldsymbol{f} + \boldsymbol{g} < C}} \langle \boldsymbol{f}, \boldsymbol{\mu} \rangle + \langle \boldsymbol{g}, \boldsymbol{\nu} \rangle$$

Here, $f + g \leq C$ is to be understood as $f_i + g_j \leq C_{ij}$ for all $i \in [m]$, $j \in [n]$. In the special case where $\mathcal{X} = \mathcal{Y}$ and C corresponds to a metric, i.e. $C_{ij} = d(x_i, y_j)$, the Wasserstein distance of order p between μ and ν for $p \in [1, \infty)$ is defined as:

$$W_p(\boldsymbol{\mu}, \boldsymbol{\nu}) = \left(\min_{\gamma \in \Pi(\boldsymbol{\mu}, \boldsymbol{\nu})} \sum_{i,j} C_{ij}^p \Gamma_{ij}\right)^{\frac{1}{p}}.$$

3.2. Entropic Optimal Transport

A common regularization of the problem consists of adding an entropic regularizer. We define entropy as follows:

Definition 3 (Entropy). For a matrix $P = [p_{ij}]_{ij} \in \mathbb{R}^{m \times n}$, we define its entropy H(P) as

$$H(P) := -\sum_{i=1}^{m} \sum_{j=1}^{n} p_{ij} (\log p_{ij} - 1)$$

if all entries are positive, and $H(P) := -\infty$ if at least one entry is negative. For entries $p_{ij} = 0$, we use the convention $0 \log 0 = 0$, as $x \log x \xrightarrow{x \to 0} 0$.

The entropic optimal transport problem is defined as follows.

Problem 4 (Entropic Optimal Transport Problem). *For* $\varepsilon > 0$, *the* entropic optimal transport problem *is defined as:*

$$L^{\varepsilon}(\boldsymbol{\mu}, \boldsymbol{\nu}) := \min_{\Gamma_{\varepsilon} \in \Pi(\boldsymbol{\mu}, \boldsymbol{\nu})} \langle C, \Gamma_{\varepsilon} \rangle - \varepsilon H(\Gamma_{\varepsilon}).$$

The term $-\varepsilon H(\Gamma_{\varepsilon})$ is referred to as the entropic regularizer, and ε as the regularizing constant.

Note that this is identical to the regular optimal transport problem, except that the regular one does not contain the regularization term $-\varepsilon H(\Gamma)$. As the objective in Problem 4 is ε -strongly convex, the problem admits a unique solution (see (Peyré & Cuturi, 2019)).

The *Gibbs kernel* is defined as $K = \exp(-C/\varepsilon)$. Then the entropic dual problem reads:

Problem 5 (Entropic Dual Problem). *The entropic dual problem is defined as:*

$$D^{\varepsilon}(\boldsymbol{\mu}, \boldsymbol{\nu}) := \max_{\boldsymbol{f}_{\varepsilon} \in \mathbb{R}^{m}, \ \boldsymbol{g}_{\varepsilon} \in \mathbb{R}^{n}} \langle \boldsymbol{f}_{\varepsilon}, \boldsymbol{\mu} \rangle + \langle \boldsymbol{g}_{\varepsilon}, \boldsymbol{\nu} \rangle - \varepsilon \left\langle e^{\boldsymbol{f}_{\varepsilon}/\varepsilon}, Ke^{\boldsymbol{g}_{\varepsilon}/\varepsilon} \right\rangle.$$

Again, without the regularization term $-\varepsilon \left\langle e^{f_\varepsilon/\varepsilon}, Ke^{g_\varepsilon/\varepsilon} \right\rangle$, this equals the regular optimal transport dual; note, however, that the unregularized dual is subject to the constraint $f+g \leq C$. The following proposition holds (see, e.g., (Peyré & Cuturi, 2019)).

Proposition 6. The unique solution of Problem 4 is given by

$$\Gamma_{\varepsilon} = diag(\mathbf{u})Kdiag(\mathbf{v})$$

for two positive scaling vectors \mathbf{u} and \mathbf{v} unique up to a scaling constant (i.e. $\lambda \mathbf{u}$, $\frac{1}{\lambda} \mathbf{v}$ for $\lambda > 0$). Furthermore, (\mathbf{u}, \mathbf{v}) are linked to the solution $(\mathbf{f}_{\varepsilon}, \mathbf{g}_{\varepsilon})$ from Problem 5 via

$$(\boldsymbol{u}, \boldsymbol{v}) = (\exp(\boldsymbol{f}_{\varepsilon}/\varepsilon), \exp(\boldsymbol{g}_{\varepsilon}/\varepsilon)).$$

A solution to the entropic dual can be approximated by a solution to the regular dual in the following sense.

Proposition 7. Let (f,g) be optimal for the unregularized dual problem and $(f^{\varepsilon}, g^{\varepsilon})$ be optimal for the regularized dual problem for some $\varepsilon > 0$. Then $(f^{\varepsilon}, g^{\varepsilon})$ is feasible for the unregularized problem, i.e. $f^{\varepsilon} + g^{\varepsilon} \leq C$, and

$$0 \le D^{\varepsilon}(\boldsymbol{\mu}, \boldsymbol{\nu}) - \left[\langle \boldsymbol{f}, \boldsymbol{\mu} \rangle + \langle \boldsymbol{g}, \boldsymbol{\nu} \rangle - \varepsilon \left\langle e^{\boldsymbol{f}/\varepsilon}, K e^{\boldsymbol{g}/\varepsilon} \right\rangle \right]$$

$$< mn\varepsilon,$$

i.e. the value the entropic dual takes at (f,g) differs from the optimal value by at most a factor of $mn\varepsilon$. In particular, if $\varepsilon \to 0$, the optimum of the entropic dual converges to its value at (f,g).

A proof can be found in the appendix.

3.3. Sinkhorn Algorithm Initializations

The Sinkhorn algorithm – see Algorithm 1 – is an iterative procedure based on the original work of Sinkhorn and Knopp (Sinkhorn & Knopp, 1967). It was first applied to the optimal transport setting in the seminal work *Sinkhorn distances: lightspeed computation of optimal transport* (Cuturi, 2013).

Algorithm 1 Sinkhorn Algorithm

```
1: in C \in \mathbb{R}^{m \times n}, \varepsilon > 0, \mu \in \Delta_{>0}^{m-1}, \nu \in \Delta_{>0}^{n-1}

2: initialize \boldsymbol{v}^0 (e.g. \boldsymbol{v}^0 \leftarrow 1_n), l \leftarrow 0, K \leftarrow \exp(-C/\varepsilon)

3: repeat

4: \boldsymbol{u}^{l+1} \leftarrow \mu ./K\boldsymbol{v}^l

5: \boldsymbol{v}^{l+1} \leftarrow \nu ./K^\top \boldsymbol{u}^{l+1}

6: l \leftarrow l+1

7: until stopping criterion is met

8: \Gamma \leftarrow \operatorname{diag}(\boldsymbol{u}^l)K\operatorname{diag}(\boldsymbol{v}^l)

9: out \Gamma, \langle C, \Gamma \rangle
```

In the algorithm, ./ is to be understood as element-wise division. Note that the algorithm requires both input distributions to be positive everywhere to prevent division by zero. As Sinkhorn and Knopp showed in their original work, the iterates u^l and v^l from the algorithm converge to the vectors u and v from Proposition 6. By the same proposition, we know that $v = \exp(q_{\varepsilon}/\varepsilon)$ for a solution q_{ε} of the regularized dual, and by Proposition 7 we know that we can approximate g_{ε} by a solution g of the unregularized dual. Hence, we can make a neural network learn such \boldsymbol{q} to initialize the Sinkhorn algorithm via $\boldsymbol{v}^0 = \exp(\boldsymbol{q}/\varepsilon)$. Furthermore, optimal (f, g) of the unregularized dual are linked via $g = f^C$, where f^C is the C-transform of f, defined via $g_j = \min_i C_{ij} - f_i$. As both f and g are Cconcave functions - meaning they are the C-transform of some other function, in this case of each other – whenever they're optimal (see (Villani, 2009)), we can also instead learn f and compute g from it via $g = f^C$. This has the advantage that in enforces C-concavity of g. In the following section, we will see how this learning is performed.

4. Learning Initializations

We will train and test the algorithm on 28×28 -dimensional images, i.e. 784-dimensional distributions. We will always use the squared euclidean distance in the unit square as the cost function for our experiments; however, other

cost functions could also be considered. Our choice yields the squared Wasserstein-2 distance as the optimal transport cost. Hyperparameter values can be found in the appendix. All code is available at https://github.com/j-geuter/SinkhornNNHybrid.

4.1. Generator

The generator is a one-layer ResNet-like network, where inputs z come from an l-dimensional Gaussian prior, $z \sim \rho_z$. The output of the generator is

$$(\boldsymbol{\mu}, \boldsymbol{\nu}) = g_{\boldsymbol{\theta}}(\boldsymbol{z}) = \lambda \text{ReLU}(T(\boldsymbol{z})) + \text{net}_{\boldsymbol{\theta}}(\boldsymbol{z}) + c,$$

where T interpolates its input to match the generator's output dimension, and λ is a constant controlling the impact of the skip connection. The network $\operatorname{net}_{\theta}$ is a single fully connected linear layer with ReLU activation. The small, positive constant c ensures that all inputs are active during training. In the end, $g_{\theta}(z)$ will be normalized such that it contains two distributions which both sum to one. The generator is universal in the following sense.

Theorem 8. Let $0 < \lambda < 1$ and $\tilde{g} : \mathbb{R}^k \to \mathbb{R}^k$ be defined via

$$\tilde{g}(z) = \lambda \text{ReLU}(z) + \text{net}_{\theta}(z),$$

where $z \sim \rho_z = \mathcal{N}(0, I)$, and where $\operatorname{net}_{\theta} : \mathbb{R}^k \to \mathbb{R}^k$ is Lipschitz continuous with $\operatorname{Lip}(\operatorname{net}_{\theta}) < \lambda$. Then \tilde{g} is Lipschitz continuous with $\operatorname{Lip}(\tilde{g}) < 1 + \lambda$, and for any $x \in \mathbb{R}^k_{\geq 0}$ it holds

$$\rho_{\tilde{g}_{\#}\rho_{\mathbf{z}}}(x) \ge \frac{(1-\lambda)^k}{(1+\lambda)^k} \mathcal{N}\left(x \left| 0, \frac{1}{(1+\lambda)^2} I \right.\right).$$

In other words, \tilde{g} has positive density at any non-negative $x \in \mathbb{R}^k_{\geq 0}$.

Proof. From Theorem 1 and Lemma 2 in (Behrmann et al., 2019), it follows that \tilde{q} is invertible with

$$\operatorname{Lip}(\tilde{g}) < 1 + \lambda, \quad \operatorname{Lip}(\tilde{g}^{-1}) < \frac{1}{1 - \lambda}.$$

Hence, as \tilde{g} is bi-Lipschitz, we have for any $x, h \in \mathbb{R}^k$:

$$\lim_{t\to 0} \frac{\|\tilde{g}(\boldsymbol{x}+t\boldsymbol{h})-\tilde{g}(\boldsymbol{x})\|}{\|t\boldsymbol{h}\|} > 0,$$

which shows that $D\tilde{g}$ is invertible on all of \mathbb{R}^k . By the inverse function theorem, it follows that $\tilde{g}^{-1} \in C^1$, i.e. \tilde{g} is a C^1 -diffeomorphism. The statement now follows from Lemma 4 in (Altekrüger et al., 2022). Note that we can ignore the inverse of the ReLU function appearing in \tilde{g}^{-1} , as we are only considering non-negative samples in the image space.

¹One could also make the network learn f_{ε} directly. However, then one is faced with the problem of having to choose a regularizing constant ε for training, while during testing, this constant might change; also, as the entropic problem is only solved approximately by the Sinkhorn algorithm, one would have to use ground truth labels for f_{ε} during training that are mere approximations. Empirically, learning f works slightly better.

Remark 9. Note that in our setting, the network $\operatorname{net}_{\theta}$ appearing in Theorem 8 has the very simple structure of a single linear layer with ReLU activation; hence, we could have also just added the densities of the two terms in \tilde{g} . However, the theorem shows that the statement is true for far more general classes of networks, and can be of independent value. Particularly, we want to mention that it can easily be extended to compositions of such ResNets.

Note that Theorem 8 is not directly applicable to our setting for two reasons: First, we add a small constant c to the generator's output. This constant ensures that all training samples are positive everywhere, and vastly improves learning speed as it ensures that all inputs are active. However, this is not restrictive of the problem, as the Sinkhorn algorithm requires inputs to be positive anyways. Second, in Theorem 8 both in- and outputs to \tilde{q} have the same dimension. This could be achieved in our setting by setting l = 2.784 = 1568, which would result in T being the identity. However, in practice, using l = 128 proved to achieve better results. This can be argued for by the manifold hypothesis (Fefferman et al., 2016), i.e. the fact that typically, datasets live on low-dimensional manifolds embedded in high-dimensional spaces. This means the input consists of two 8 × 8 images, one for each of the two output distributions, and T interpolates each of them to have dimension 28×28 resp.

By Remark 9, we do not have to enforce constraints on the Lipschitz constant of net_{θ} in order to ensure that our generator has positive density at any non-negative sample. However, in the setting of a more complex ResNet, Lipschitz continuity could be enforced as outlined in (Behrmann et al., 2019).

In Figure 1, images generated by g after no training, training on 50k unique samples, and training on 100k unique samples are shown.

4.2. Approximator

The approximator is a three-layer fully connected network, where the first layer has $2\cdot 784\text{-}\text{dimensional}$ in- and $6\cdot 784\text{-}\text{dimensional}$ output, the second layer has $6\cdot 784\text{-}\text{dimensional}$ in- and output, and the last layer has $6\cdot 784\text{-}\text{dimensional}$ in- and 784-dimensional output. The first two layers contain ReLU activations and batch normalizations, while the last layer has neither.

4.3. Training

As we have seen before, our training objective is

$$\max_{\boldsymbol{\theta}} \min_{\boldsymbol{\phi}} \mathbb{E}_{\boldsymbol{z} \sim \rho_{\boldsymbol{z}}} \left[\text{MSE} \left(h_{\boldsymbol{\phi}}(g_{\boldsymbol{\theta}}(\boldsymbol{z})), \boldsymbol{f}_{g(\boldsymbol{z})} \right) \right],$$

where $f_{g(z)}$ denotes a dual potential of the sample $(\mu, \nu) = g(z)$. Note that it does not have a θ subscript, because this

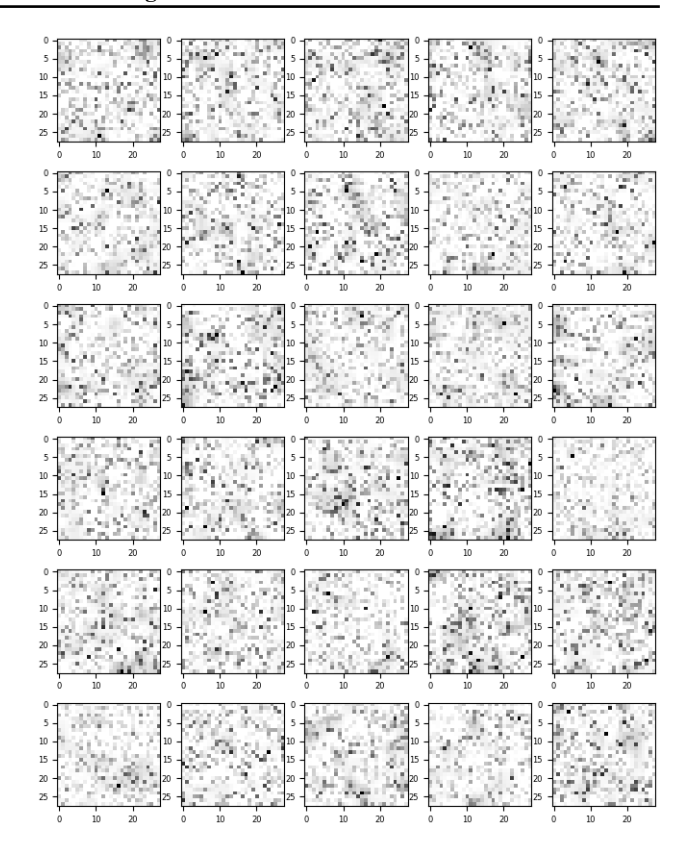


Figure 1. Generated images after no training (top two rows), training on 50k unique samples (middle two rows), and on 100k unique samples (bottom two rows), for 5 epochs resp. For all three, the first row corresponds to μ and the second row to ν .

is the target value and we do not backpropagate through it.

Furthermore, as discussed in Section 3, optimal potentials (f,g) are C-transforms of one another. Hence, if the network's output of (μ,ν) is f, its output of (ν,μ) should be f^C . This allows us to easily double the available training data. Additionally, it drives the network towards being more "C-symmmetric" in its inputs. Another property of the optimal transport dual is that its value is invariant under adding a constant to f and subtracting it from g; cf. (Peyré & Cuturi, 2019). Hence, to make learning more stable, we will only consider dual potentials that sum to 0. The training algorithm can be seen in Algorithm 2. In practice, we use the Adam optimizer for updating parameters.

De facto, z in Algorithm 2 will contain a batch of samples. DualPotential denotes any algorithm that computes a dual potential for the unregularized problem; in practice, we use ot.emd from the POT package (Flamary et al., 2021). Also, as computing these potentials is the most expensive part of the algorithm, we let each batch of samples run through h_{ϕ} for multiple epochs. During each such epoch, all samples in the batch are shuffled randomly and fed to h_{ϕ}

Algorithm 2 Training Algorithm

```
1: in cost C \in \mathbb{R}^{n \times n}, prior \rho_z, learning rates \alpha, \beta, epochs
  2: for i = 1, 2, ... until stopping criterion do
  3:
                  z \leftarrow \text{sample}(\rho_z)
  4:
                  (\boldsymbol{\mu}, \boldsymbol{\nu}) \leftarrow g_{\boldsymbol{\theta}}(\boldsymbol{z})
                  f \leftarrow \text{DualPotential}((\mu, \nu), C)
   5:
                 oldsymbol{f} \leftarrow oldsymbol{f} - rac{\sum_i oldsymbol{f}_i}{n} for e=1,2,..., epochs do
   6:
  7:
                         f_{\star} \leftarrow h_{\phi}((\mu, \nu))
  8:
                        \begin{aligned} \phi &\leftarrow \phi - \alpha_i \nabla_{\phi} \text{MSE}(\boldsymbol{f_{\star}}, \boldsymbol{f}) \\ \boldsymbol{f_{\star}^C} &\leftarrow h_{\phi}((\boldsymbol{\nu}, \boldsymbol{\mu})) \\ \phi &\leftarrow \phi - \alpha_i \nabla_{\phi} \text{MSE}(\boldsymbol{f_{\star}^C}, \boldsymbol{f}^C) \end{aligned}
  9:
10:
11:
12:
                  \theta \leftarrow \theta + \beta_i \nabla_{\theta} MSE(f_{\star}, f)
13:
14: end for
```

in minibatches.

5. Experiments

In all plots in this section, we will always plot the 95% confidence intervals alongside the mean values; however, oftentimes, the confidence intervals are too narrow to be visible.

5.1. Test Sets

We test the network on four different test datasets. The first one is generated by assigning each point in the distribution a random value (see the appendix for more details), the second one consists of teddy bears from the Google Quick, Draw! dataset, the third one is MNIST, and the last one a greyscale version of CIFAR10. Figure 2 shows the test datasets.

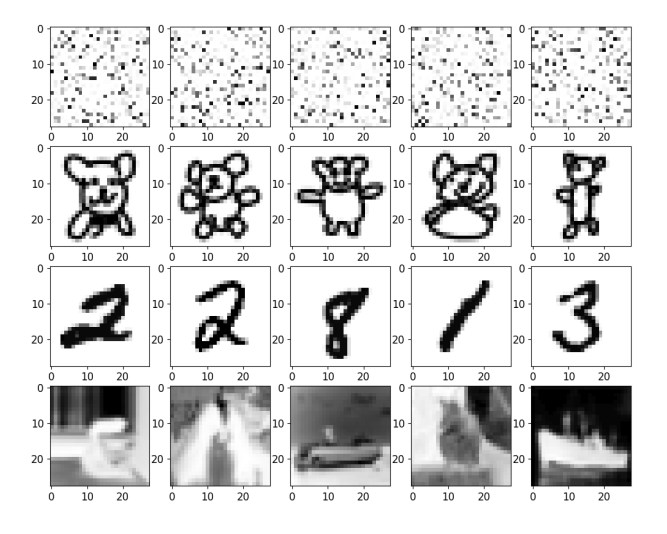


Figure 2. Test datasets 'random', 'teddies', 'MNIST' and 'CIFAR'.

5.2. Loss Function Comparison

As discussed in Section 2, (Amos et al., 2022) use a loss on the transport distance. In Figure 3, we can see how training compares to our loss function.²

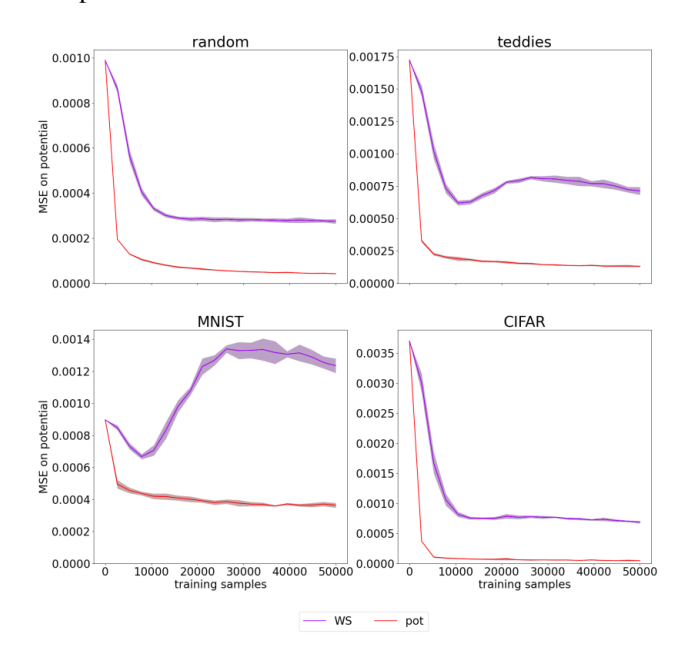


Figure 3. Comparison of loss functions on the transport distance ('WS') vs. on the potential ('pot').

5.3. Initialization Performance

We compare the Sinkhorn algorithm convergence for our learned initialization to the default one (i.e. $1_{28} \in \mathbb{R}^{28}$). We initialize it as outlined in section 3.3; however, to prevent entries from being too small or two large, we bound v^0 from below by 1e-35 and from above by 1e35. This means for input measures μ and ν , we set

$$v^0 \leftarrow \max\left\{1e\text{-}35, \min\left\{1e35, \exp(h_\phi(\boldsymbol{\mu}, \boldsymbol{\nu})^C/\varepsilon)\right\}\right\}.$$

The network is trained on 100.000 unique training samples, each of which is trained on epochs = 5 times. Training takes just over 3 hours on a NVIDIA Telsa T4 GPU with 16 GB; however, we note that almost all training time is needed to compute ground truth potentials with ot.emd. In all experiments, we set $\varepsilon=0.00025$. Figures 4 and 5 show the relative error on the transport distance, with respect to the number of Sinkhorn iterations and the computation time resp. As one can see from the figures, the two plots look very similar; this is because the time needed to compute the initialization vector is negligible compared to the time needed by the Sinkhorn algorithm.

²In this figure, the number of samples on the x-axis refers to the number of unique samples multiplied by the number of epochs.

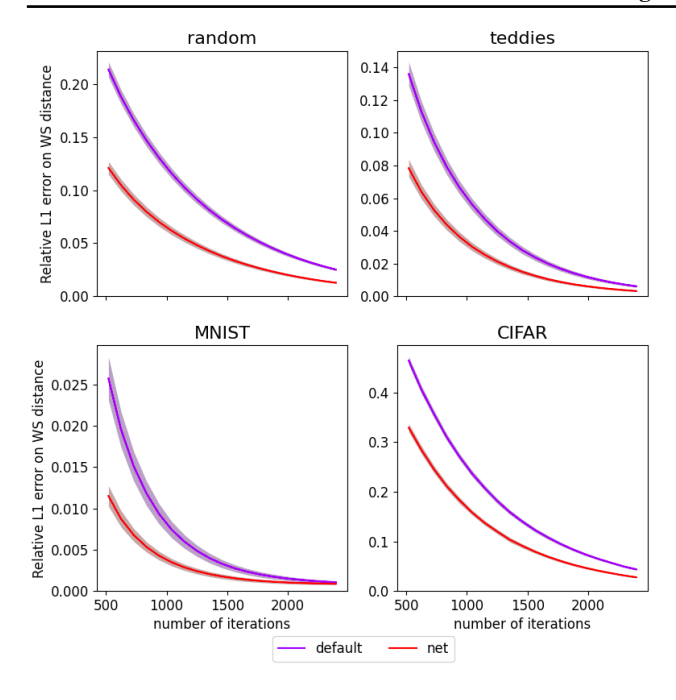


Figure 4. Relative errors on the transport distances w.r.t. the number of Sinkhorn iterations.

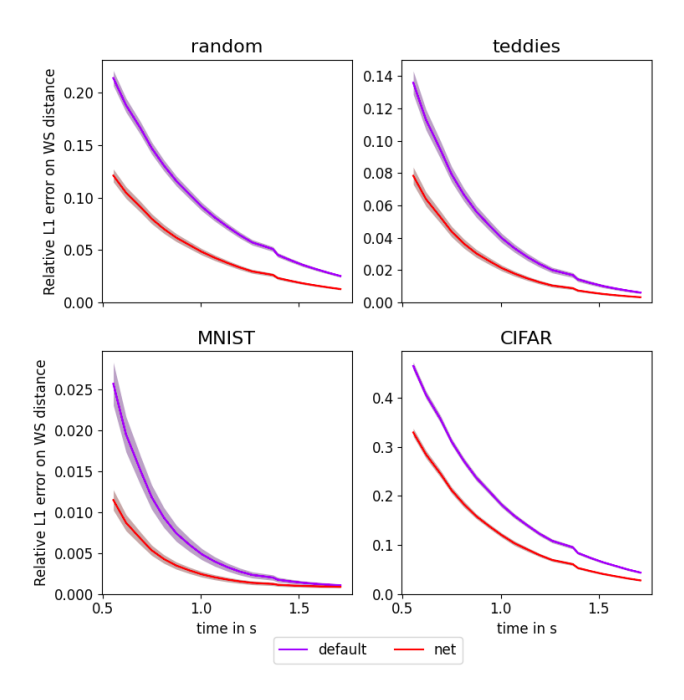


Figure 5. Relative errors on the transport distances w.r.t. computation time.

However, in practice, one does not have access to the true transport distances, hence a loss on the marginal constraint violations (MCV) is oftentimes used as a stopping criterion for the Sinkhorn algorithm. The MCV measure how

far the plan $\Gamma^{\varepsilon}_{(l)}$ computed by the Sinkhorn algorithm after l iterations is from fulfilling the marginal constraints $1_m^{\top}\Gamma^{\varepsilon}_{(l)}=\boldsymbol{\nu}^{\top}$ and $\Gamma^{\varepsilon}_{(l)}1_n=\boldsymbol{\mu}$. Different flavours to measure the MCV exist; we use

$$\frac{\left(\left\|\mathbf{1}_{m}^{\top}\Gamma_{(l)}^{\varepsilon}-\boldsymbol{\nu}^{\top}\right\|_{1}\right)+\left(\left\|\Gamma_{(l)}^{\varepsilon}\mathbf{1}_{n}-\boldsymbol{\mu}\right\|_{1}\right)}{2}.$$

The average marginal constraint violation can be seen in Figure 6. Tables 1 and 2 show the average number of iterations to achieve 1e-2 and 1e-3 marginal constraint errors.³

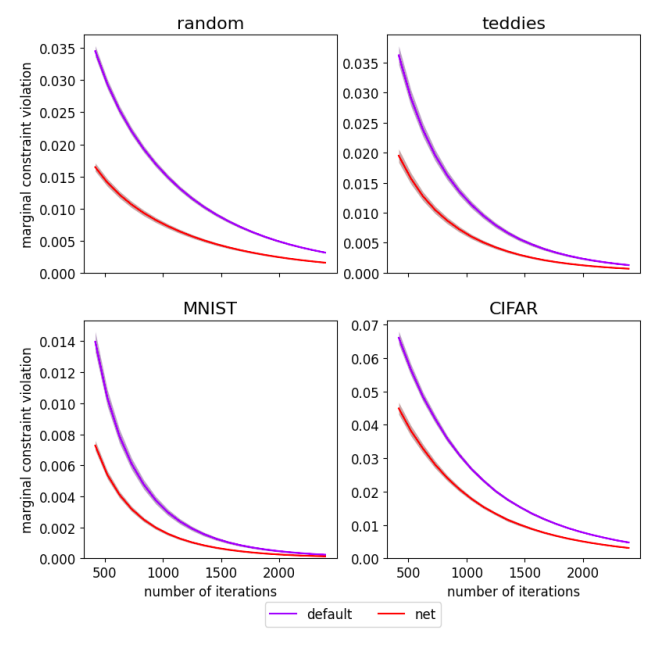


Figure 6. Average marginal constraint violations.

	default	net
random	3355 ± 38	2725 ± 52
teddies	2473 ± 48	2067 ± 49
MNIST	1528 ± 32	1225 ± 23
CIFAR	3555 ± 36	3195 ± 34

Table 1. Avg. number of iterations needed to achieve a 1e-3 MCV.

	default	net
random	1330 ± 29	755 ± 41
teddies	1083 ± 30	735 ± 39
MNIST	528 ± 17	322 ± 10
CIFAR	1738 ± 20	1422 ± 29

Table 2. Avg. number of iterations needed to achieve a 1e-2 MCV.

³Measured with an accuracy of 25 Sinkhorn iterations.

5.4. Wasserstein Barycenters

Wasserstein barycenters are barycenters with respect to the Wasserstein distance. Namely, a Wasserstein barycenter of measures $\{\nu_1, ..., \nu_n\}$ is any measure μ such that

$$\mu = \underset{\mu'}{\operatorname{arg\,min}} \sum_{i=1}^{n} W_{p}^{p}(\mu', \nu_{i}).$$

By duality, we can compute this as

$$oldsymbol{\mu} = rg\min_{oldsymbol{\mu'}} \sum_{i=1}^n \langle oldsymbol{f}_i, oldsymbol{\mu'}
angle + \langle oldsymbol{g}_i, oldsymbol{
u}_i
angle$$

for solutions (f_i, g_i) of the dual problem of μ' and ν_i with cost function d^p . In this section, we have a look at how Wasserstein barycenters can be computed using only the approximator.

Usually, the dual potential approximations of the approximator are not accurate enough to use them on their own, hence we used them to initialize the Sinkhorn algorithm. However, in applications such as barycenter computations, where the potentials are integrated with respect to the measures, some of the approximation errors tend to cancel out: Assume the true potential is f and the network's approximation of it is $f + \sigma$, where $\sigma_i \sim Z_i$ with $\mathbb{E}[Z_i] = 0$, then

$$\mathbb{E}_{m{\sigma}}[\langle m{f}+m{\sigma},m{\mu}
angle] = \langle m{f},m{\mu}
angle + \mathbb{E}_{m{\sigma}}\left[\sum_i m{\sigma}_im{\mu}_i
ight] = \langle m{f},m{\mu}
angle.$$

In Figure 7, we can see the barycenters of 20 samples for each of the digits 0, 2, 5, and 7 from the MNIST dataset, computed with the network only. They were computed using a simple gradient descent with respect to μ' on the sum

$$\sum_{i=1}^n \langle oldsymbol{f}_i, oldsymbol{\mu'}
angle + \langle oldsymbol{g}_i, oldsymbol{
u}_i
angle.$$

6. Summary

We showed that it is possible to learn universal initializations to the Sinkhorn algorithm via the optimal transport dual problem. We used a two-network approach, where one network is used to generate training samples for the second network. Both networks are trained in an adversarial manner similar to GANs. We proved that the generating network is universal in that it can produce any pair of distributions as training data. When comparing the convergence speed of the Sinkhorn algorithm for its default initialization vs. the network initialization,

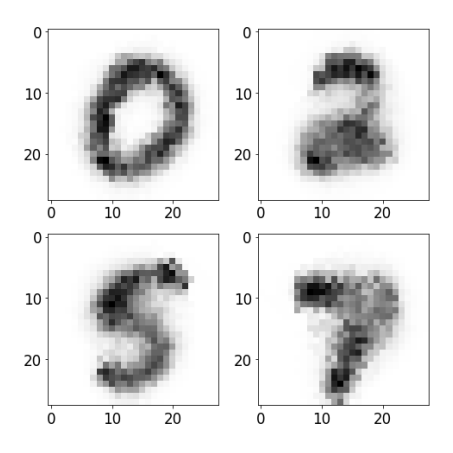


Figure 7. Barycenters of 20 MNIST samples for the digits 0, 2, 5, and 7, computed using only the approximator.

the network initialization significantly outperforms the default initialization on all test datasets, showing that it can generalize to before unseen datasets. This is true both when considering relative errors on the transport distance, as well as for the marginal constraint violations. To achieve a marginal constraint violation error of 1e-3, the network initialization needs 16% less iterations averaged over all test datasets; to achieve an error of 1e-2, it needs 33% less iterations on average, and even up to 43\% less depending on the dataset, almost doubling convergence speed. The network is easy to train and universal as it successfully generalizes to arbitrary datasets, and the computation time needed to compute the initialization is negligible compared to the time needed by the Sinkhorn algorithm. Hence, we propose initializing the Sinkhorn algorithm using such a network.

Acknowledgements

The authors would like to thank Paul Hagemann for very insightful discussions, particularly regarding the generator. Furthermore, we thank Nicolas Courty for helpful comments and ideas on how to train the approximator.

References

Altekrüger, F., Denker, A., Hagemann, P., Hertrich, J., Maass, P., and Steidl, G. PatchNR: Learning from Very Few Images by Patch Normalizing Flow Regularization, 2022. URL https://arxiv.org/abs/2205.12021.

Alvarez-Melis, D. and Fusi, N. Dataset Dynamics via Gradient Flows in Probability Space. In Meila, M. and Zhang, T. (eds.), Proceedings of the 38th International Conference on Machine Learning, volume 139 of Proceedings of Machine Learning Research, pp. 219–230. PMLR, 18–

⁴Which is, of course, a simplification of the true approximation error.

- 24 Jul 2021. URL https://proceedings.mlr.press/v139/alvarez-melis21a.html.
- Alvarez-Melis, D., Schiff, Y., and Mroueh, Y. Optimizing Functionals on the Space of Probabilities with Input Convex Neural Networks. *Transactions on Machine Learning Research*, 2022. URL https://openreview.net/forum?id=dpOYN708Jm.
- Amos, B., Xu, L., and Kolter, J. Z. Input Convex Neural Networks. In Precup, D. and Teh, Y. W. (eds.), *Proceedings of the 34th International Conference on Machine Learning*, volume 70 of *Proceedings of Machine Learning Research*, pp. 146–155. PMLR, 06–11 Aug 2017. URL https://proceedings.mlr.press/v70/amos17b.html.
- Amos, B., Cohen, S., Luise, G., and Redko, I. Meta Optimal Transport, 2022. URL https://arxiv.org/abs/2206.05262.
- Arjovsky, M., Chintala, S., and Bottou, L. Wasserstein Generative Adversarial Networks. In Precup, D. and Teh, Y. W. (eds.), *Proceedings of the 34th International Conference on Machine Learning*, volume 70 of *Proceedings of Machine Learning Research*, pp. 214–223. PMLR, 06–11 Aug 2017. URL https://proceedings.mlr.press/v70/arjovsky17a.html.
- Behrmann, J., Grathwohl, W., Chen, R. T. Q., Duvenaud, D., and Jacobsen, J.-H. Invertible Residual Networks. *Proceedings of the International Conference on Machine Learning*, 2019. doi: 10.48550/ARXIV.1811.00995. URL https://arxiv.org/abs/1811.00995.
- Benamou, J.-D. and Brenier, Y. A computational fluid mechanics solution to the Monge-Kantorovich mass transfer problem. *Numerische Mathematik*, 84:375–393, 2000.
- Bunne, C., Krause, A., and Cuturi, M. Supervised Training of Conditional Monge Maps, 2022a. URL https://arxiv.org/abs/2206.14262.
- Bunne, C., Papaxanthos, L., Krause, A., and Cuturi, M. Proximal Optimal Transport Modeling of Population Dynamics. In *Proceedings of The 25th International Conference on Artificial Intelligence and Statistics*, volume 151 of *Proceedings of Machine Learning Research*, pp. 6511–6528. PMLR, 28–30 Mar 2022b. URL https://proceedings.mlr.press/v151/bunne22a.html.
- Courty, N., Flamary, R., Habrard, A., and Rakotomamonjy, A. Joint distribution optimal transportation for domain adaptation. In *Advances in Neural Information Processing Systems*, volume 30, 2017. URL https://proceedings.

- neurips.cc/paper/2017/file/ 0070d23b06b1486a538c0eaa45dd167a-Paper. pdf.
- Courty, N., Flamary, R., and Ducoffe, M. Learning Wasserstein Embeddings. In *ICLR 2018 6th International Conference on Learning Representations*, pp. 1–13, Vancouver, Canada, April 2018. URL https://hal.inria.fr/hal-01956306.
- Cuturi, M. Sinkhorn Distances: Lightspeed Computation of Optimal Transport. In Burges, C., Bottou, L., Welling, M., Ghahramani, Z., and Weinberger, K. (eds.), Advances in Neural Information Processing Systems, volume 26. Curran Associates, Inc., 2013. URL https://proceedings.neurips.cc/paper/2013/file/af21d0c97db2e27e13572cbf59eb343d-Paper.pdf.
- Dadashi, R., Hussenot, L., Geist, M., and Pietquin, O. Primal Wasserstein Imitation Learning, 2020. URL https://arxiv.org/abs/2006.04678.
- Dinh, L., Krueger, D., and Bengio, Y. NICE: Non-linear Independent Components Estimation. In *ICLR Workshop*, 2015.
- Engquist, B. and Yang, Y. Seismis imaging and optimal transport. *Communications in Information and Systems*, 19(2):95–145, 2019. URL https://www.intlpress.com/site/pub/pages/journals/items/cis/content/vols/0019/0002/a001/index.php.
- Fefferman, C., Mitter, S., and Narayanan, H. Testing the manifold hypothesis. *Journal of the American Mathematical Society*, 29(4):983–1049, 2016. URL https://www.ams.org/journals/jams/2016-29-04/S0894-0347-2016-00852-4/.
- Flamary, R., Courty, N., Gramfort, A., Alaya, M. Z., Boisbunon, A., Chambon, S., Chapel, L., Corenflos, A., Fatras, K., Fournier, N., Gautheron, L., Gayraud, N. T., Janati, H., Rakotomamonjy, A., Redko, I., Rolet, A., Schutz, A., Seguy, V., Sutherland, D. J., Tavenard, R., Tong, A., and Vayer, T. POT: Python Optimal Transport. *Journal of Machine Learning Research*, 22(78):1–8, 2021. URL http://jmlr.org/papers/v22/20-451.html.
- Frogner, C., Zhang, C., Mobahi, H., Araya, M., and Poggio, T. A. Learning with a Wasserstein Loss. In *Advances in Neural Information Processing Systems*, volume 28. Curran Associates, Inc., 2015. URL https://proceedings.neurips.cc/paper/2015/file/a9eb812238f753132652ae09963a05e9-Paper.pdf.

- Galichon, A. Optimal Transport Methods in Economics. Princeton University Press, 2016.
- Goodfellow, I., Pouget-Abadie, J., Mirza, M., Xu, B., Warde-Farley, D., Ozair, S., Courville, A., and Bengio, Y. Generative Adversarial Nets. In Ghahramani, Z., Welling, M., Cortes, C., Lawrence, N., and Weinberger, K. (eds.), Advances in Neural Information Processing Systems, volume 27. Curran Associates, Inc., 2014. URL https://proceedings.neurips.cc/paper/2014/file/5ca3e9b122f61f8f06494c97b1afccf3-Paper.pdf.
- Gracyk, A. and Chen, X. GeONet: a neural operator for learning the Wasserstein geodesic, 2022. URL https://arxiv.org/abs/2209.14440.
- He, K., Zhang, X., Ren, S., and Sun, J. Deep Residual Learning for Image Recognition. In 2016 IEEE Conference on Computer Vision and Pattern Recognition (CVPR), pp. 770–778, 2016. doi: 10.1109/CVPR.2016.90.
- Kingma, D. P. and Welling, M. Auto-Encoding Variational Bayes. In *Proceedings of the 2nd International Conference on Learning Representations*, 2014. doi: 10.48550/ARXIV.1312.6114. URL https://arxiv.org/abs/1312.6114.
- Kobyzev, I., Prince, S. J., and Brubaker, M. A. Normalizing Flows: An Introduction and Review of Current Methods. *IEEE Transactions on Pattern Analysis and Machine Intelligence*, 43(11):3964–3979, 2021. doi: 10.1109/TPAMI.2020.2992934.
- Kolouri, S., Park, S. R., Thorpe, M., Slepcev, D., and Rohde, G. K. Optimal Mass Transport: Signal processing and machine-learning applications. *IEEE Signal Processing Magazine*, 34(4):43–59, 2017. doi: 10.1109/MSP.2017. 2695801.
- Papamakarios, G., Nalisnick, E., Rezende, D. J., Mohamed, S., and Lakshminarayanan, B. Normalizing Flows for Probabilistic Modeling and Inference. Journal of Machine Learning Research, 22(57):1–64, 2021. URL http://jmlr.org/papers/v22/19-1028.html.
- Peyré, G. and Cuturi, M. Computational Optimal Transport: With Applications to Data Science. *Foundations and Trends® in Machine Learning*, 11(5-6):355–607, 2019. ISSN 1935-8237. doi: 10.1561/2200000073. URL http://dx.doi.org/10.1561/2200000073.
- Rezende, D. and Mohamed, S. Variational inference with normalizing flows. In Bach, F. and Blei, D. (eds.), *Proceedings of the 32nd International Conference on Machine Learning*, volume 37 of *Proceedings of Machine*

- Learning Research, pp. 1530–1538, Lille, France, 07–09 Jul 2015. PMLR. URL https://proceedings.mlr.press/v37/rezende15.html.
- Schiebinger, G., Shu, J., Tabaka, M., Cleary, B., Subramanian, V., Solomon, A., Gould, J., Liu, S., Lin, S., Berube, P., Lee, L., Chen, J., Brumbaugh, J., Rigollet, P., Hochedlinger, K., Jaenisch, R., Regev, A., , and Lander, E. S. Optimal-Transport Analysis of Single-Cell Gene Expression Identifies Developmental Trajectories in Reprogramming. *Cell*, 176(4):928–943, 2019.
- Schmitz, M. A., Heitz, M., Bonneel, N., Ngolè, F., Coeurjolly, D., Cuturi, M., Peyré, G., and Starck, J.-L. Wasserstein Dictionary Learning: Optimal Transport-Based Unsupervised Nonlinear Dictionary Learning. *SIAM Journal on Imaging Sciences*, 11(1):643–678, jan 2018. doi: 10.1137/17m1140431. URL https://doi.org/10.1137%2F17m1140431.
- Sinkhorn, R. and Knopp, P. Concerning nonnegative Matrices and doubly stochastic Matrices. *Pacific Journal of Mathematics*, 21(2), 1967.
- Sohl-Dickstein, J., Weiss, E., Maheswaranathan, N., and Ganguli, S. Deep Unsupervised Learning using Nonequilibrium Thermodynamics. In Bach, F. and Blei, D. (eds.), Proceedings of the 32nd International Conference on Machine Learning, volume 37 of Proceedings of Machine Learning Research, pp. 2256–2265, Lille, France, 07–09 Jul 2015. PMLR. URL https://proceedings.mlr.press/v37/sohl-dickstein15.html.
- Song, Y. and Ermon, S. Generative Modeling by Estimating Gradients of the Data Distribution. In Wallach, H., Larochelle, H., Beygelzimer, A., d'Alché-Buc, F., Fox, E., and Garnett, R. (eds.), *Advances in Neural Information Processing Systems*, volume 32. Curran Associates, Inc., 2019. URL https://proceedings.neurips.cc/paper/2019/file/3001ef257407d5a371a96dcd947c7d93-Paper.pdf.
- Thornton, J. and Cuturi, M. Rethinking Initialization of the Sinkhorn Algorithm, 2022. URL https://arxiv.org/abs/2206.07630.
- Villani, C. Optimal Transport Old and New. Springer, 2009.
- Zhang, C., Cai, Y., Lin, G., and Shen, C. DeepEMD: Few-Shot Image Classification With Differentiable Earth Mover's Distance and Structured Classifiers. In 2020 IEEE/CVF Conference on Computer Vision and Pattern Recognition (CVPR), pp. 12200–12210, 2020. doi: 10.1109/CVPR42600.2020.01222.

A. Theory Background

Proof of Proposition 7. In this proof we will write ε as superscripts. Let Γ^{ε} be the solution of the entropic primal problem. As we have

$$1 \geq \Gamma_{ij}^{\varepsilon} = e^{(\boldsymbol{f}_{i}^{\varepsilon} + \boldsymbol{g}_{j}^{\varepsilon} - C_{ij})/\varepsilon} \text{ for all } i \in [\![m]\!], \ j \in [\![n]\!],$$

it follows that $f_i^{\varepsilon} + g_j^{\varepsilon} - C_{ij} \leq 0$ for all i and j, i.e. $f^{\varepsilon} + g^{\varepsilon} \leq C$. This makes $(f^{\varepsilon}, g^{\varepsilon})$ feasible for the unregularized dual. From optimality of (f, g) we get

$$\langle oldsymbol{f}, oldsymbol{\mu}
angle + \langle oldsymbol{g}, oldsymbol{
u}
angle \geq \langle oldsymbol{f}^arepsilon, oldsymbol{\mu}
angle + \langle oldsymbol{g}^arepsilon, oldsymbol{
u}
angle.$$

This gives us

$$\begin{split} &D^{\varepsilon}(\boldsymbol{\mu},\boldsymbol{\nu}) - \left[\langle \boldsymbol{f},\boldsymbol{\mu} \rangle + \langle \boldsymbol{g},\boldsymbol{\nu} \rangle - \varepsilon \langle e^{\boldsymbol{f}/\varepsilon},Ke^{\boldsymbol{g}/\varepsilon} \rangle \right] \\ = &\langle \boldsymbol{f}^{\varepsilon},\boldsymbol{\mu} \rangle + \langle \boldsymbol{g}^{\varepsilon},\boldsymbol{\nu} \rangle - \varepsilon \langle e^{\boldsymbol{f}^{\varepsilon}/\varepsilon},Ke^{\boldsymbol{g}^{\varepsilon}/\varepsilon} \rangle - \left[\langle \boldsymbol{f},\boldsymbol{\mu} \rangle + \langle \boldsymbol{g},\boldsymbol{\nu} \rangle - \varepsilon \langle e^{\boldsymbol{f}/\varepsilon},Ke^{\boldsymbol{g}/\varepsilon} \rangle \right] \\ \leq &\varepsilon \left[\langle e^{\boldsymbol{f}/\varepsilon},Ke^{\boldsymbol{g}/\varepsilon} \rangle - \langle e^{\boldsymbol{f}^{\varepsilon}/\varepsilon},Ke^{\boldsymbol{g}^{\varepsilon}/\varepsilon} \rangle \right] \\ \leq &\varepsilon \sum_{i,j} e^{(\boldsymbol{f}_i + \boldsymbol{g}_j - C_{ij})/\varepsilon} \leq mn\varepsilon, \end{split}$$

where in the last step we used the fact that $f + g \le C$. Also note that the starting expression is always greater or equal to 0 by optimality of $(f^{\varepsilon}, g^{\varepsilon})$.

B. Training Details

Hyperparameters. In the generator, we set $\lambda=0.3$ and c=1e-2. The learning rate for the generator is set to 0.2352 initially, while the approximator's learning rate starts at 2.352. Both are updated via

$$\alpha_i \leftarrow 0.99 \cdot \alpha_{i-1}$$

 $\beta_i \leftarrow 0.99 \cdot \beta_{i-1}$.

The batches are of size 500, and each minibatch of size 100. The number of epochs is set to 5.

Test datasets. For the 'random' test dataset, each pixel was assigned a value r^3 , where r is a random number between 0 and 1, before the distributions where normalized. Additionally, for each sample in all test datasets, a small constant was added to the distribution before normalization such that they did not contain any zeros.

Code. All code used for experiments is available at https://github.com/j-geuter/SinkhornNNHybrid.